Magnetic crossover in the one-dimensional Hubbard model in the presence of a magnetic field

2001 J. Phys.: Condens. Matter 13 6759

(http://iopscience.iop.org/0953-8984/13/31/313)

INSTITUTE OF PHYSICS PUBLISHING JOURNAL OF PHYSICS: CONDENSED MATTER

J. Phys.: Condens. Matter **13** (2001) 6759–6772 PII: S0953-8984(01)21606-3

Magnetic crossover in the one-dimensional Hubbard model in the presence of a magnetic field

A N Kocharian, Nicholas Kioussis and S H Park

Department of Physics and Astronomy, California State University, Northridge, CA 91330-8268, USA

Received 23 February 2001, in final form 4 May 2001
Published 19 July 2001
Online at stacks.iop.org/JPhysCM/13/6759

Abstract

The ground-state (GS) properties of the one-dimensional (1D) Hubbard model at half-filling are examined in the presence of a magnetic field using the generalized mean-field (GMF) approach, which includes the spin-density and the electron–hole correlations on an equal footing. The GMF formalism provides insight into both the metal–insulator transition and the transition from itinerant to localized magnetism with applied field. The GMF theory can differentiate the energy gap from the antiferromagnetic order parameter in the presence of a magnetic field. The numerical results for the GS energy, the magnetization, the spin susceptibility, and the number of doubly occupied sites are in good agreement with the exact results over a wide range of U/t and h/t. The calculated h–U phase diagram exhibits a magnetic crossover from itinerant electron–hole pairs to a Bose–Einstein condensate state of local pairs. The overall picture of the magnetic crossover in 1D is found to be similar for the simple case of constant density of states, putting the GMF approach on a firmer basis in two and three dimensions.

1. Introduction

The repulsive Hubbard Hamiltonian is the simplest model that includes the basic ingredients of electron correlations for the treatment of the metal–insulator transition and magnetism [1–8]. The model displays the many-body physics responsible for the interplay between the Mott–Hubbard localization and antiferromagnetism, and is currently a subject of intensive study due to its possible relevance in high-T_c superconductivity [9]. The intermediate-coupling regime ($U \sim t$) is of particular interest, as in this range of parameters, the competition between band effects and localization due to correlations is important. So far, the ground-state (GS) properties of the Hubbard model have been solved exactly only in one and infinite dimensions (D) [11, 12], including the presence of a magnetic field [13–15]. The continuum model for a similar excitonic insulator [16–20], consisting of spinless particles and holes with equal masses and interacting via an attractive delta-function potential, has been solved also exactly in 1D [21, 22].

0953-8984/01/316759+14$30.00

The lack of exact results in higher dimensions has stimulated the growth of numerical calculations on finite systems, through exact-diagonalization techniques [10, 23], quantum Monte Carlo (QMC) simulations, and renormalization group (RG) techniques [24, 25], which are limited to finite-size systems. Furthermore, a variety of approximate analytical approaches have been used to study the Hubbard model, including mean-field theories [26–31], Green function decoupling schemes [32], functional integral formulations [33], and variational approaches [34, 35].

The exact solution for the Hubbard model in one dimension [11, 13–15, 21, 22] provides a test of the quality of the different approximate theories, especially in the intermediate-coupling region $U \sim t$.

The purpose of this work is to apply the generalized mean-field (GMF) treatment, which includes the spin magnetization and the antiferromagnetic correlations on an equal footing, to study the GS properties of the Hubbard chain at half-filling in the presence of a magnetic field, and to compare the results with the Bethe-*ansatz* solutions.

We find that the GS properties are in qualitative, and in some cases quantitative, agreement with the exact results over a wide range of U/t and h. The GMF approach also correctly predicts the presence of a gap as $U \to 0$ over the entire range of h, consistent with the exact results [3, 11], and it becomes exact for $h \geqslant h_c$, where h_c is the upper critical magnetic field for a fully polarized state.

Finally, we investigate the interplay between itinerant and local magnetism through the calculation of the $\vec{k}$-dependent single-particle energy gap $E_{gap}(k)$ in the presence of a magnetic field. The GMF approach differentiates the energy gap from the antiferromagnetic order parameter at relatively high fields or strong coupling, giving rise to a magnetic crossover. The calculated h–U phase diagram exhibits three regimes. Simply stated, we find that k_F increases with h from $k_F = \pi/2$ at $h = 0$ to $k_F = \pi$ at $h_0(U)$, where $h_0(U)$ is the lower critical field, above which the single-particle energy gap occurs at $k_F = \pi$. In the weak-magnetic-field regime, $h \leqslant h_0(U)$, we have itinerant magnetism with reduced local moment and the antiferromagnetic order parameter $\Delta_{Q=\pi} = E_{gap}(k_F)$, with $k_F < \pi$. With increasing h or U/t, the system undergoes a smooth transition from itinerant electron–hole pairs to local Bose–Einstein pairs with zero momentum. For $h_0 \leqslant h \leqslant h_c$, there is a phase with well developed local moments, an energy gap at $k_F = \pi$, and $E_{gap} > \Delta$. Finally, for $h \geqslant h_c(U)$, we have a fully polarized phase.

The paper is organized as follows. In section 2 we present the GMF formalism and describe the crossover from itinerant to localized magnetism. Also in this section we present analytical results for the GS properties for the simple case of constant density of states. In section 3, we present results for the number of doubly occupied sites, the effective bandwidth, and the zero-field susceptibility and compare them with the exact Bethe-*ansatz* results in the absence of an external magnetic field. Section 4 presents the GMF results for the GS properties, the energy gap, and the phase diagram in the presence of a magnetic field. A concluding summary follows in section 5.

2. GMF formalism

2.1. GMF Model

The Hubbard model in one dimension and in the presence of a magnetic field h is

$$H = -t \sum_{i\sigma} (c^{+}_{i\sigma} c_{i+1\sigma} + c^{+}_{i+1\sigma} c_{i\sigma}) + U \sum_{i} c^{+}_{i\uparrow} c^{+}_{i\downarrow} c_{i\downarrow} c_{i\uparrow} - \frac{h}{2} \sum_{i} (c^{+}_{i\uparrow} c_{i\uparrow} - c^{+}_{i\downarrow} c_{i\downarrow}) \tag{1}$$

where $c^+_{i\sigma}$ and $c_{i\sigma}$ are the creation and annihilation operators for the electron with spin σ at site i, $t > 0$ is the matrix element for hopping between nearest-neighbour sites, U is the on-site Coulomb interaction, and the third term is the Zeeman energy in the presence of a magnetic field H, $h = g\mu_B H$ [13, 14].

In this work we generalize the mean-field approach [27–29] in the presence of a magnetic field, by introducing two order parameters: an antiferromagnetic order parameter

$$\Delta_Q = \frac{2U}{N}\sum_k \langle c^+_{k+Q\downarrow} c_{k\uparrow}\rangle \tag{2}$$

describing the electron–hole correlations or the transverse (x–y) antiferromagnetic spin fluctuations ($\langle s^+\rangle = \langle s^-\rangle = \Delta_Q/2U$) [8]; and the spin magnetization along the z-direction

$$s^z = \frac{1}{2N}\sum_j \langle c^+_{j\uparrow} c_{j\uparrow} - c^+_{j\downarrow} c_{j\downarrow}\rangle. \tag{3}$$

In the case of particle–hole symmetry, where $\epsilon_k = -\epsilon_{k+\pi}$, the value of $\boldsymbol{Q}$ minimizing the energy is $\boldsymbol{Q} = \pi$ ($\Delta \equiv \Delta_{Q=\pi}$), and the GS energy reduces to

$$E_{GS} = -\frac{1}{N}\sum_k \sqrt{\left(\epsilon_k - \frac{\overline{h}}{2}\right)^2 + \frac{\Delta^2}{4}} + \frac{\Delta^2}{4U} + Us^2 + \frac{U}{4} \tag{4}$$

where $\overline{h} = h + 2sU$.

The bipartite 1D Hubbard model (N even) can be reinterpreted in terms of electron–hole pairs through the electron–hole transformation for the electron operators for one species such as $c^+_{i\downarrow} = c^+_{i\downarrow}$ and $c^+_{i\uparrow} = (-1)^i c_{i\uparrow}$ [31]. In the two-orbital model of spinless fermions with intra-site attraction [21, 22], the parameter $\bar{\mu} = \mu + U\bar{n}/2 = -\overline{h}/2$ plays the role of a renormalized chemical potential for the electron–hole pair concentration $\bar{n} = 1 - 2s$ within the attractive Hubbard model.

Minimization of E_{GS} with respect to Δ and s gives the system of self-consistent equations

$$\Delta = \frac{U}{2N}\sum_k \frac{\Delta}{\sqrt{(\epsilon_k - \overline{h}/2)^2 + \Delta^2/4}} \tag{5}$$

$$s = -\frac{1}{2N}\sum_k \frac{(\epsilon_k - \overline{h}/2)}{\sqrt{(\epsilon_k - \overline{h}/2)^2 + \Delta^2/4}}. \tag{6}$$

For $h \geqslant h_c$, $s = 1/2$ and $\Delta = 0$, and the GMF gives the exact critical field, $h_c = \sqrt{16t^2 + U^2} - U$, for a fully saturated state [6].

The density of doubly occupied sites $D(h)$, measuring the degree of electron correlation, is

$$\frac{1}{N}\sum_i [\langle n_{i\downarrow}\rangle\langle n_{i\uparrow}\rangle + \langle c^+_{i\uparrow} c_{i\downarrow}\rangle\langle c^+_{i\downarrow} c_{i\uparrow}\rangle] = D_0(h) - \frac{\Delta^2(h)}{4U^2}. \tag{7}$$

Here, $D_0(h) = \langle n_\uparrow\rangle\langle n_\downarrow\rangle = \frac{1}{4} - s^2(h)$ is the number of doubly occupied sites in the presence of a magnetic field at $U = 0$. The ratio $\Delta^2(h)/4U^2$, which describes the average density of bound electron–hole pairs (excitons), decreases at the expense of the number of doubly occupied sites. Using the Feynman–Hellmann theorem, the effective kinetic energy is

$$t_{eff} = -\frac{t}{N}\sum_{\langle i,j\rangle,\sigma} \left\langle c^+_{i\sigma} c_{i\sigma}\right\rangle = E_{GS} - UD.$$

2.2. Magnetic crossover

In this section we investigate the crossover associated with the evolution of the single-particle energy gap with h and U/t. The single-particle energy gap is

$$E_{gap}(\boldsymbol{k}_F) = \sqrt{(2\epsilon_{\boldsymbol{k}_F} - \overline{h})^2 + \Delta^2}. \tag{8}$$

In figure 1, we show a schematic picture of the evolution of the single-particle energy spectrum at relatively weak and strong magnetic field. For $h = 0$ the gap occurs at $k_F = \pi/2$ and is identical to the order parameter ($E_{gap} = \Delta$) for all values of U/t. With increasing $h > 0$, k_F increases with h according to

$$k_F = \begin{cases} \cos^{-1}\left(-\dfrac{\overline{h}}{4t}\right) & \text{if } |\overline{h}| < 4t \\ \pi & \text{if } |\overline{h}| \geqslant 4t. \end{cases} \tag{9}$$

The lower critical field $h_0 \leqslant h_c$, at which the energy gap occurs at $k_F = \pi$, can be determined from $4t - 2Us(U, h_0) - h_0 = 0$. For $h \leqslant h_0(U)$, $k_F < \pi$ and $E_{gap}(k_F) \equiv \Delta$, while for $h \geqslant h_0(U)$, $k_F = \pi$ and $E_{gap}(\pi) = \sqrt{[(4t - \overline{h})^2 + \Delta^2]} \geqslant \Delta$. This variation of E_{gap} with h suggests a transition from itinerant electron–hole pairs with local moment $m \approx 1/2$ ($m \equiv 1 - 2D$) for $h \leqslant h_0$, into a Bose condensate regime of localized pairs with $k_F = \pi$ and $m \approx 1$. Note that when h increases, $\bar{\mu}$ decreases, approaching the bottom of the conduction band ($-2t$) at $\bar{k}_F = 0$. This transition is analogous to that in superconductivity, where there is a crossover from an itinerant BCS to a Bose condensate regime ($\bar{k}_F = 0$) of electron pairs [36–41]. Although the results presented in section 4 use the tight-binding model ($\epsilon_k = -2t \cos k$), we present below simple analytical expressions for the GS properties for the simple case of constant density of states.

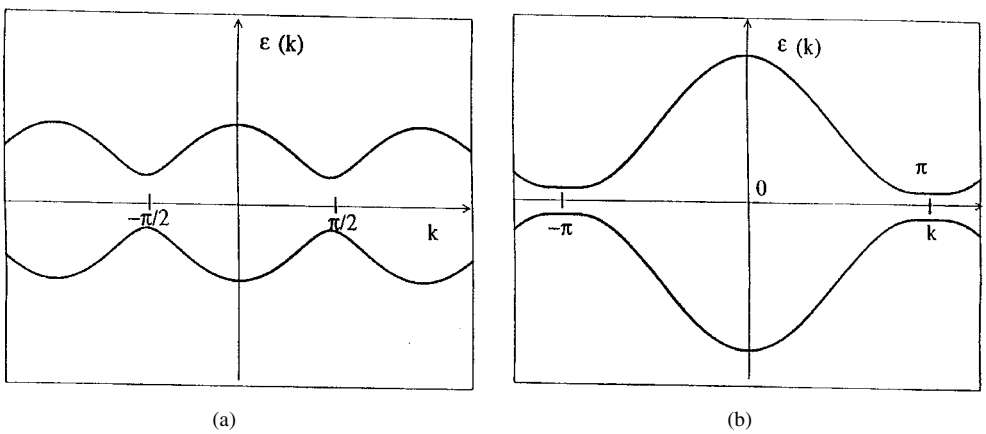

(a) (b)

Figure 1. The GMF excitation spectrum for (a) $h < h_0$, where the gap occurs at $k_F < \pi$, and for (b) $h_0 < h < h_c$, where the gap occurs at $k_F \equiv \pi$.

2.3. Constant density of states

For the case of constant density of states with bandwidth $W = 2zt$, equations (4)–(6) can be solved analytically for any dimension $d = z/2$. At half-filling, the two self-consistent equations for Δ and s reduce to

$$\Delta = 4zt\sqrt{1 - 4s^2} \Big/ \sinh \frac{4zt}{U} \tag{10}$$

$$\overline{h} = 8szt \coth \frac{4zt}{U}. \tag{11}$$

Note that $\Delta \to 0$ as $s \to 1/2$, indicating an excitonic instability near magnetic saturation. Equation (11) gives a magnetization $s = h/(2h_c)$ and a magnetic susceptibility

$$\chi = g\mu_B \frac{\mathrm{d}s}{\mathrm{d}H} = g^2\mu_B^2/2h_c$$

where

$$h_c = 4zt \coth \frac{4zt}{U} - U.$$

The GMF susceptibility increases monotonically with $U/4zt$ and is larger than the exact result [14]. Increase of dimensionality leads to a decrease of χ by factor of $(2d)^{-2}$. The GS energy, $E_{GS} = -h_c(\frac{1}{4} - s^2)$, reduces to $E_{GS} = 0.25h_c$ at $h = 0$, in good agreement with the exact result $E_{GS} = \alpha h_c$, where $\alpha \sim 0.3$–0.4 [11]. For $U/4zt \ll 1$, $E_{GS} \approx -zt + U/2$ and for $U/4zt \gg 1$, $E_{GS} \approx -4z^2t^2/U$. The double occupancy

$$D = \left(\frac{1}{4} - s^2\right)\left(1 - \frac{16z^2t^2}{U^2 \sinh^2(4zt/U)}\right)$$

reduces to $D = 4z^2t^2/3U^2$ in the strong-coupling limit, in qualitative agreement with the exact result. The single-particle gap at h_c is

$$E_{gap} = -4zt + U + h_c = 4zt\left(\coth \frac{4zt}{U} - 1\right) \tag{12}$$

and the lower critical field $h_0(U)$ is

$$h_0 = 4zt - Us = 4zt - U \tanh \frac{4zt}{U}. \tag{13}$$

For $h > h_c$, the GMF gap increases with $U/2W$, in agreement with the exact result. In the weak-coupling regime, $E_{gap} \sim 8zt\mathrm{e}^{-8zt/U}$, compared to the exact expression $E_{gap} \sim U^2/2zt$ [14]. However, for $U/4zt \geqslant 1$, $E_{gap} = U - 4zt - 16t^2z^2/3U$, which correctly predicts the appearance of the linear t-term in the exact solution [14]. Overall, even in the simple case of constant density of states, the GMF approach captures qualitatively the GS properties of the Hubbard model.

3. Ground-state properties at $h = 0$

In figure 2(a) we present the GMF results (dashed curve) for the double occupancy as a function of U/t and compare them with the exact ones (solid curve). In the weak-coupling regime, the GMF expression overestimates the double occupancy

$$D_0 - D = \frac{64t^2\mathrm{e}^{-4\pi t/U}}{U^2}$$

compared to the exact expression

$$D_0 - D = \frac{7U\zeta(3)}{2t\pi^2}$$

due to the underestimation of electron correlations. On the other hand, in the strong-coupling regime, the GMF approach overestimates electron correlations giving $D = 4t^2/U^2$ compared to the exact expression of $D = 4t^2 \ln 2/U^2$. In figure 2(b) we plot the GMF results (dashed

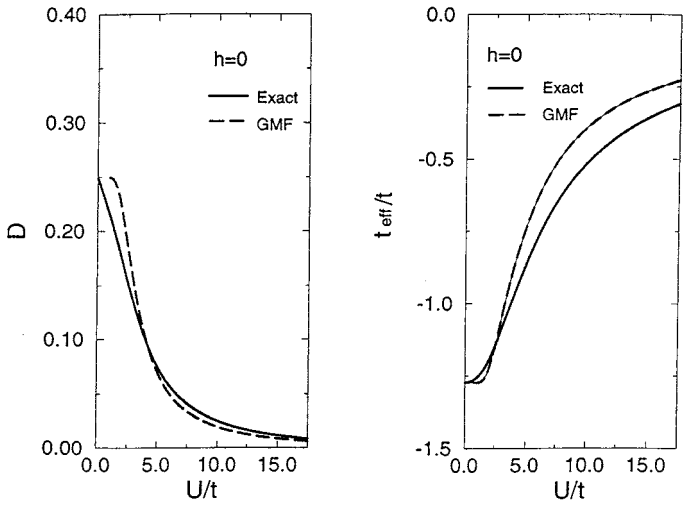

Figure 2. (a) Zero-field double occupancy versus U/t in the GMF approach (dashed curve) along with the exact results (solid curve). (b) Zero-field effective kinetic energy versus U/t in the GMF approach (dashed curve) compared to the exact results (solid curve).

curve) for t_{eff} versus U/t along with the exact results (solid curve). The GMF approach overestimates the effective kinetic energy

$$t_{eff} = \frac{4t}{\pi} - \frac{64t^2 e^{-4\pi t/U}}{U}$$

for $U/t \leqslant 1$ (the exact result is $t_{eff} = 4t/\pi - 7U^2\zeta(3)/[4\pi^2 t]$), while it underestimates $t_{eff} \approx 4t^2/U$ in the strong-coupling limit. Overall, there is good agreement between the GMF and the exact results for t_{eff} over a wide range of h and U/t.

In figure 3 we show the GMF and the exact results [14] for the zero-field susceptibility as a function of U/t. The susceptibility increases monotonically with U/t from its initial Pauli value $\chi = g^2\mu^2/4\pi t$ for $U = 0$, to its Heisenberg value

$$\chi = \frac{g^2\mu^2 U}{16t^2}$$

for $U/t \gg 1$. In the weak-coupling regime, the GMF result reduces to

$$\chi = \frac{g^2\mu^2}{4\pi t}\left(1 + \frac{U}{2\pi t}\right)$$

where the first-order correction term is smaller than the exact one by a factor of two [14].

4. Ground-state results at $h \neq 0$

4.1. GMF order parameters

The variations of s and Δ with h are shown in figures 4 and 5, respectively. In figure 4 we also present the exact results for the magnetization for $U/t = 3$ and 10. The GMF approach overestimates the magnetization over the entire parameter space (U/t and $h \leqslant h_c$), due to the neglect of spin fluctuations. The magnetization approaches its saturated value more rapidly as U/t increases, consistent with the zero-field susceptibility $\chi(h)$ in figure 3. For $h \leqslant h_c(U)$,

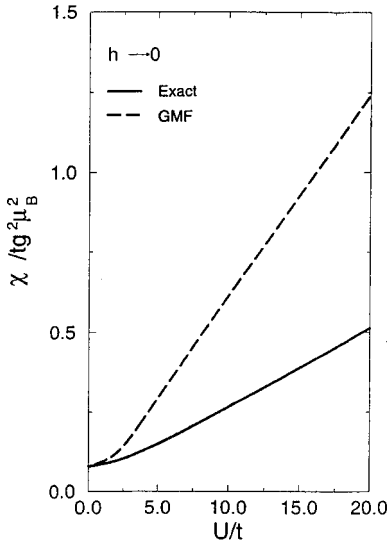

Figure 3. Zero-field susceptibility $\chi(U)/tg^2\mu_B{}^2$ as a function of U/t obtained using the GMF approach (dashed curve) along with the exact results (solid curve).

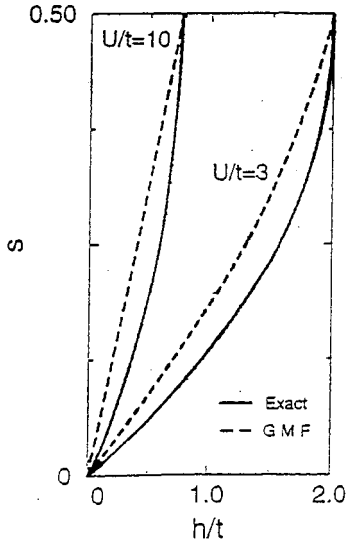

Figure 4. Magnetization $s(h)$ versus h/t in the GMF approach (dashed curve) along with the exact results (solid curve), for $U/t = 3$ and 10.

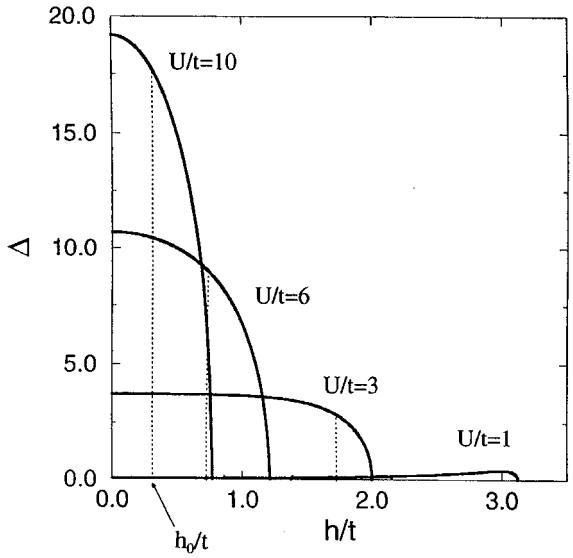

Figure 5. Antiferromagnetic order parameter $\Delta(h)$ as a function of h/t, for $U/t = 1, 3, 6$, and 10.

the non-zero value of Δ shows the stability of the antiferromagnetic insulating state. The parameter Δ varies non-monotonically with h for $U/t \leqslant 1$. As $h \to h_c(U)$, $s \to 1/2$, whereas $\Delta = U\sqrt{(1-4s^2)} \to 0$, indicating the suppression of the transverse magnetization $\langle s^+ \rangle = \Delta/2U$ by h. Figures 4 and 5 suggest three different phases: a 'pure' antiferromagnetic state at $h = 0$ ($\Delta \neq 0$, $s \equiv 0$); a mixed phase ($\Delta \neq 0$ and $s \neq 0$) for $h \leqslant h_c(U)$; and a fully saturated magnetic state for $h \geqslant h_c$ ($\Delta \equiv 0$ and $s \equiv 1/2$). The behaviour of s with field resembles that of valence with applied pressure in the mixed-valence state [20].

4.2. Ground-state energy

The variation of E_{GS} with s is shown in figure 6 for two values of U/t, along with the exact results of Takahashi [13]. The GS energy increases monotonically with U/t and h, and reduces to

$$E_{GS} = -\frac{4}{\pi}\sqrt{1-\left(\frac{h}{h_c}\right)^2}$$

for $U = 0$. For $h = 0$ and $U/t \gg 1$, the kinetic energy is suppressed due to U, and the GS energy reduces to $E_{GS} = 4t^2/U$, i.e. the energy of the 1D Heisenberg model [1]. Near saturation, $E_{GS} = -(1/2 - s)(\sqrt{[U^2 + 16t^2]} - U)$ increases linearly with s.

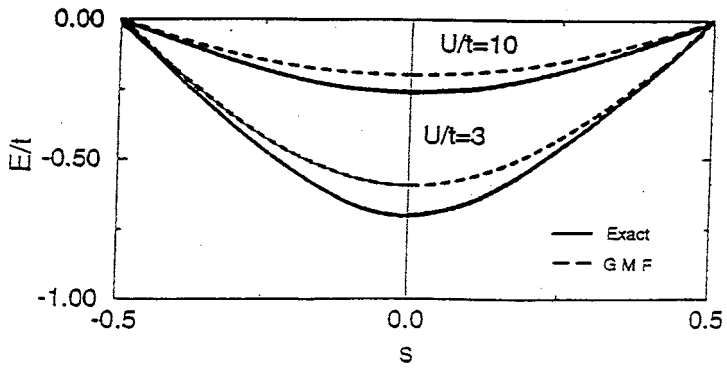

Figure 6. Ground-state energy $E(s)$ versus magnetization s (dashed curve) compared to the exact result (solid curve) for $U/t = 3$ and 10.

4.3. Magnetic susceptibility

The results for $\chi(h)$ as a function of h are shown in figure 7, for $U/t = 3$, 6, and 10. While the exact expression for the susceptibility exhibits a Van Hove singularity, $\chi \sim 1/\sqrt{(h_c - h)}$, as $h \to h_c$ (or $s \to 1/2$), the GMF approach yields a finite susceptibility. Thus, the GMF overestimates χ for small h and underestimates it as $h \to h_c$. For $h > h_c$, $\chi = 0$, as in the exact case. As expected, the GMF approach does not describe well physical quantities which involve charge or spin excitations.

4.4. Double occupancy

The double occupancy $D(h)$ is plotted versus h in figure 8 for $U/t = 3$, 6, and 10. Also we show in the figure the corresponding exact results for D at $h = 0$ and at $h = h_c$ for $U = 3$ (crosses), 6 (circles), and 10 (triangles). The exact expression

$$\frac{\mathrm{d}D}{\mathrm{d}h} \sim -\frac{1}{\sqrt{h_c - h}}$$

exhibits a Van Hove singularity as $h \to h_c$, whereas the GMF yields a finite slope for all values of U/t. While the effect of U is to increase both Δ and s for $h \neq 0$, the effect of h is to increase s but to decrease Δ. However, the combined effect of U/t and h/t on s and Δ leads to a monotonic decrease of $D(h)$, in agreement with the exact result. The decrease of D leads to the enhancement of the local moment. For $U/t \ll 1$, the local moment approaches

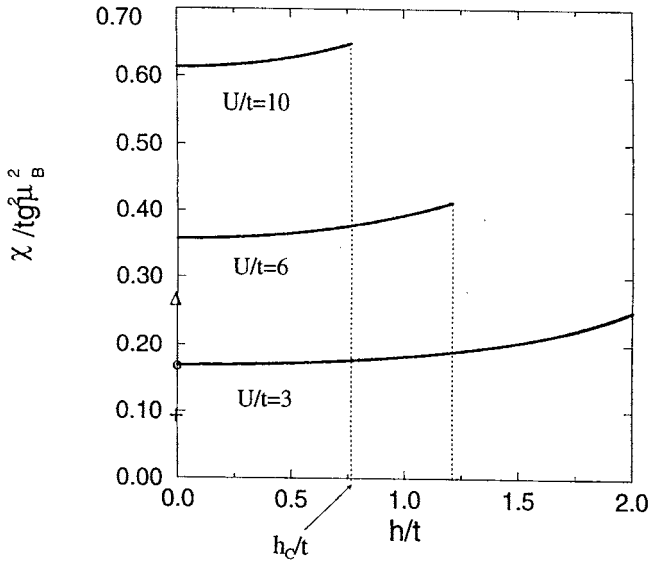

Figure 7. Susceptibility $\chi(h)/tg^2\mu_B{}^2$ as a function of magnetic field for $U/t = 3$, 6, and 10. The crosses, circles, and triangles denote the exact values of χ at $h/t = 0$ for $U/t = 3$, 6, and 10. The exact critical field for a fully saturated magnetic state is denoted by h_c.

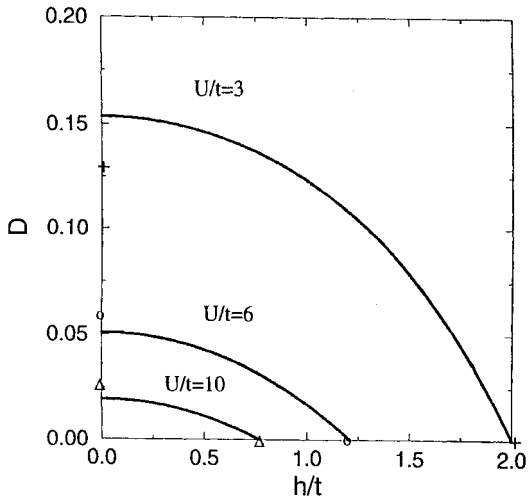

Figure 8. Double occupancy $D(h)$ as a function of h for $U/t = 3$, 6, and 10. The crosses, circles, and triangles denote the exact values of $D(h)$ at $h/t = 0$ and $h = h_c$ for $U/t = 3$, 6, and 10.

saturation $m \approx 1$ at relatively high h ($h_0 \approx h_c$). In contrast, for large U/t, where D is small, the transition in the local magnetic regime occurs at relatively weak field, $h_0 \ll h_c$.

4.5. Kinetic energy

In figure 9, we plot the variation of t_{eff} versus h for $U/t = 3$, 6, and 10. Also shown in figure 9 are the exact results for the effective kinetic energy at $h = 0$ and at $h = h_c$ for

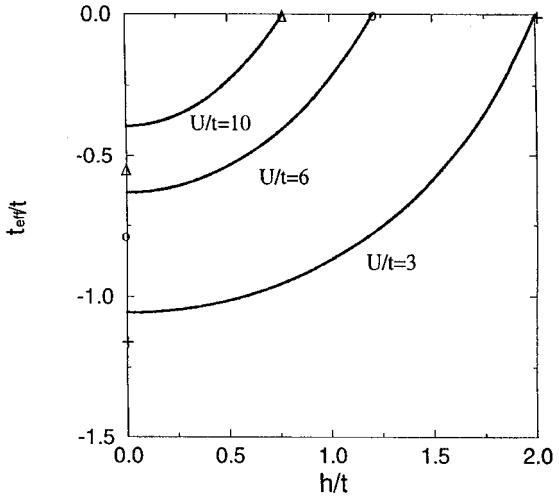

Figure 9. Effective kinetic energy $t_{eff}(h)/t$ versus h/t for $U/t = 3$, 6, and 10. The crosses, circles, and triangles denote the exact values of $t_{eff}(h)/t$ at $h = 0$ and $h = h_c$, respectively for $U/t = 3$, 6, and 10.

$U = 3$ (crosses), 6 (circles), and 10 (triangles). The GMF approach gives a finite $\mathrm{d}t_{eff}/\mathrm{d}h$ as $h \to h_c$, while the exact result shows a square-root singularity. For $U/t \geqslant 3$, the GMF approach overestimates correlations and suppresses t_{eff} throughout the entire h-region. For $U/t \leqslant 3$, the GMF approach underestimates (overestimates) correlations for small (large) h. Overall, the GMF results are in good agreement with the exact ones.

At h_c, t_{eff} is equivalent to the kinetic energy $E(K) = \sqrt{g^2(t, K) + U^2} + 2\mu_0$ [6] of the centre of mass of the electron–hole pair in the dilute electron–hole density limit ($\bar{n} \to 0$), where $g(t, K) = -2t \cos K/2$, and $\mu_0 = -h_c/2 + U/2$. The value of K minimizing E_{GS} is $K = 0$, corresponding to the condensation of the electron–hole pairs with zero momentum. The effective *pair* hopping at $h = h_c$ is

$$t_{eff}^{(2)} \equiv \left.\frac{\partial^2 E(K)}{\partial K^2}\right|_{K=0} = 2t^2/\sqrt{16t^2 + U^2}$$

and decreases with U/t. For $U/t \leqslant 1$, the single-particle hopping reduces to $2t_{eff}$, which differs from the GMF result by a factor $2/\pi$ at $h = 0$. However, in the large-U/t limit the single-particle hopping term, $2t_0 = 2t^2/U$, is identical to the effective bandwidth at $h = 0$. The average effective radius of the bound electron–hole pair at h_c is

$$\varsigma = \sqrt{\bar{r}^2} = \frac{1}{\sqrt{2}\ln(4t/h_c)}.$$

4.6. Energy gap

In figure 10 we present the variation of the order parameter Δ and the single-particle energy gap, E_{gap}, with h for $U/t = 10$. Δ, which contains both the charge and spin excitations, is identical to the single-particle energy gap, which occurs at $k_F < \pi$, for $h < h_0$. For $h > h_0$, $E_{gap}(\pi) \geqslant \Delta$ (equation (8)). The order parameter Δ decreases with h due to the suppression of the antiferromagnetic spin fluctuations. The open circles in figure 10 denote the exact values of the Mott–Hubbard gap at $h = 0$ and $h = h_c$. At $h = h_c$, $\Delta = 0$ and the GMF gap is identical

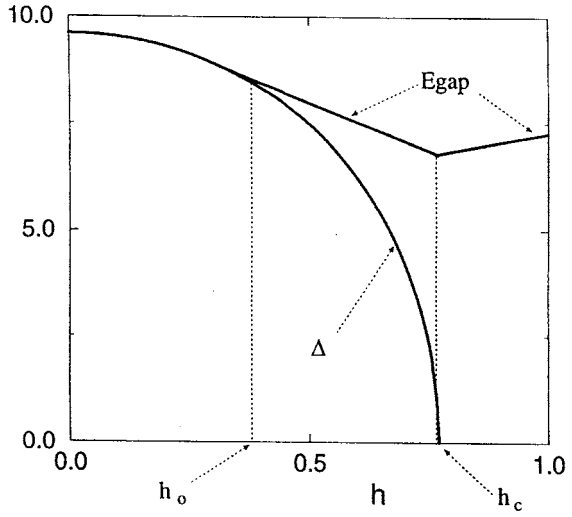

Figure 10. Energy gap E_{gap}/t and the order parameter Δ as functions of magnetic field for $U/t = 10$. Also we show the lower critical field h_0 below which $E_{gap} = \Delta$, and the upper critical field h_c at which $\Delta = 0$.

to the exact gap $E_{gap} = \sqrt{(16t^2 + U^2)} - 4t$. For $h \leqslant h_c$, the exact gap increases slowly with h, whereas the GMF gap decreases with h.

The GMF energy gap is plotted versus h/t in figure 11 for various values of U/t. We also show in this figure the exact values for the Mott–Hubbard gap at $h = 0$ and at $h = h_c$ for $U/t = 3$ (crosses), 6 (circles), and 10 (triangles). While the exact gap increases with

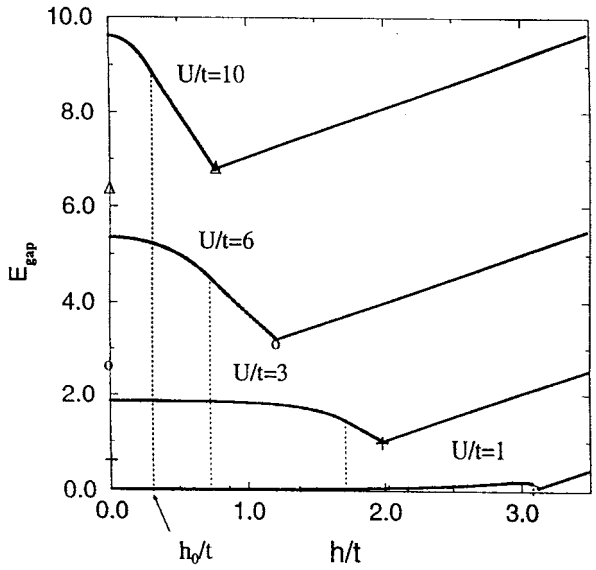

Figure 11. Energy gap E_{gap}/t versus h for $U/t = 1$, 3, 6, and 10. The crosses, circles, and triangles denote the exact values for the gap at $h = 0$ and at $h = h_c$, for $U/t = 1$, 3, and 6, respectively. Also shown is the lower critical field h_0 below which $E_{gap} = \Delta$.

increasing U/t or h/t, the GMF gap increases with U/t and decreases with h/t for $h < h_c$. For $h \geqslant h_c$, the GMF gap is identical to the exact gap and increases linearly with h. Although the GMF method overestimates the exact gap, it correctly displays the partial separation of charge and spin excitations for $h_0 \leqslant h \leqslant h_c$.

The repulsive Hubbard model ($U > 0$) at half-filling in the presence of h is equivalent to the attractive Hubbard model ($U < 0$) for general electron–hole concentration, $\bar{n} \equiv 1-2s$, with a renormalized chemical potential $\bar{\mu} \equiv -\bar{h}/2$. Correspondingly, the variation of E_{gap} versus h for the electron system is analogous to the variation of $\bar{E}_{gap}(\bar{n})$ versus particle concentration, $\bar{n}$, for the attractive Hubbard model ($U < 0$) [39,41]. That is, for the electron–hole system, $\bar{E}_{gap}(\bar{k}_F = 0) \neq \bar{\Delta}_0$, when $\bar{\mu}$ crosses the bottom of the band, $\bar{\mu} < -2t$. Here, $\bar{\Delta}_0$ is the BCS order parameter for pairing with zero centre-of-mass momentum $Q = 0$. These results indicate a transition for the exciton system from itinerant electron–hole pairs for $\bar{n} \geqslant \bar{n}_0$ into a Bose condensate regime of localized pairs with $\bar{k}_F = 0$ for $\bar{n} < \bar{n}_0$, analogous to the BCS–Bose condensate transition of electron pairs in superconductivity [36–41].

4.7. h–U phase diagram

In figure 12 we present the h–U phase diagram which exhibits three different phases: a fully saturated magnetic state (I) with $s = 1/2$ and $\Delta = 0$ for $h \geqslant h_c(U)$; a state (II) with $0 \leqslant s \leqslant 1/2$, characterized by $E_{gap}(k_F) \neq \Delta$ and $k_F = \pi$, for $h_0 \leqslant h \leqslant h_c$; and an itinerant state (III) characterized by $E_{gap}(k_F) = \Delta$, with $k_F \neq \pi$ for $h < h_0$. The crossover from itinerant to local magnetism is smooth as a function of U/t and h/t.

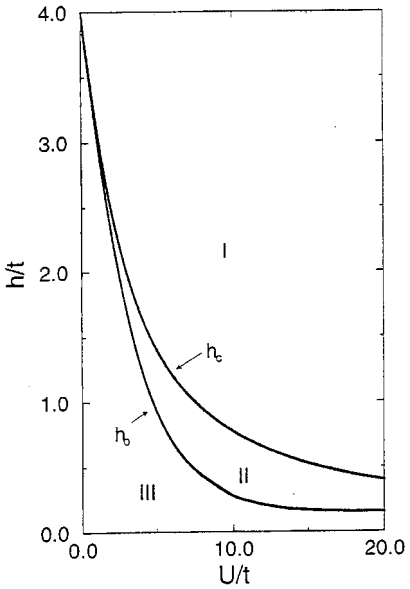

Figure 12. The U–h phase diagram. The curves labelled $h_0(U)$ and $h_c(U)$ denote the lower and upper critical fields, respectively. Phase I corresponds to a fully saturated magnetic state; in phase II ($h_0 < h < h_c$) the gap occurs at $k_F = \pi$ and $\Delta \neq E_{gap}(k_F)$ and in phase III ($0 < h < h_0(U)$) $\Delta = E_{gap}(k_F)$ and $k_F < \pi$.

As discussed earlier, phase II consists of local electron–hole pairs with zero centre-of-mass momentum. While for $U = 0$ there is a smooth transition from I into III at $h_c = h_0 = 4t$, the application of h for any infinitesimal U/t results in a transition from phase I to II. At $h = 0$,

independent of the value of U/t, there is no crossover to phase II, due to the overlap of the electron–hole pairs. The critical magnetization $h_0(U)$ along the boundary between phases II and III for the electron system maps into the critical concentration $\bar{n}_0(U) = 1 - 2s_0$, for the electron–hole system ($U < 0$), below which the system undergoes a Bose condensation with the density of excitons $\bar{\Delta}_0^2/4U^2$ [39].

5. Summary

In conclusion, the GMF approach provides a qualitative, and in some cases quantitative, description of the GS properties of the one-dimensional Hubbard model in the presence of a magnetic field. The magnetic field suppresses spin fluctuations and increases the longitudinal magnetization s. In contrast, the Coulomb interaction suppresses charge fluctuations and increases both E_{gap} and s. Overall, the GMF results for the GS properties are in good agreement with the exact results over a wide range of values of h and U/t. At $h \geqslant h_0$ we find a separation between the spin (Δ) and charge (E_{gap}) degrees of freedom, which in turn gives rise to a magnetic crossover from itinerant electron–hole pairs with small local moments to a Bose condensate regime with local moments $m \approx 1$. For $h \geqslant h_c(U)$, the gap E_{gap} increases linearly with h, in agreement with exact results. We have derived analytical expressions for the simple case of constant density of states. The overall picture of the magnetic crossover is found to be independent of the details of the electronic structure. The good agreement between the GMF results and the exact ones puts the GMF approach on a firmer basis in two and three dimensions, where the effect of fluctuations is weaker. Work currently in progress is aimed at applying the GMF approach to generalized versions of Hubbard-like models and to higher dimensions, where exact results are lacking.

Acknowledgments

The research was supported by the NSF under Grants Nos DMR-9531005 and DMR-0097187, the US Army under Grants Nos DAAG55-97-1-0093 and DAAD19-00-1-0049, the Parsons Foundation, and the Office of Research and Sponsored Projects at California State University, Northridge.

References

[1] Anderson P W 1952 *Phys. Rev.* **86** 694
[2] Krishnamurthy H R, Jayaprakash C, Sarker S and Wenzel W 1990 *Phys. Rev. Lett.* **64** 950
[3] van Dongen P G and Janis V 1994 *Phys. Rev.* **72** 3258
[4] Strack R and Vollhardt D 1994 *Phys. Rev.* **72** 3425
[5] Li Q P and Joynt R 1993 *Phys. Rev.* B **47** 3979
Li Q P and Joynt R 1994 *Phys. Rev.* B **49** 1632
[6] Kocharian A N and Sebold J 1996 *Phys. Rev.* B **53** 12 804
[7] Kocharian A N, Jermakian A K and Sogomonian A 1997 *Physica* B **230–232** 1031
[8] Kioussis N, Kocharian A N and Park S 1998 *J. Magn. Magn. Mater.* **177–181** 575
[9] Schrieffer J R, Wen X-G and Zhang S-C 1988 *Phys. Rev. Lett.* **60** 944
Schrieffer J R, Wen X-G and Zhang S-C 1989 *Phys. Rev.* B **39** 11 663
[10] Dagotto E 1994 *Rev. Mod. Phys.* **66** 763
[11] Lieb E and Wu F 1968 *Phys. Rev. Lett.* **20** 1445
[12] Georges A and Kotliar G 1996 *Rev. Mod. Phys.* **68** 13
[13] Takahashi M 1969 *Prog. Theor. Phys.* **42** 1098
[14] Takahashi M 1970 *Prog. Theor. Phys.* **43** 1619
Takahashi M 1972 *Prog. Theor. Phys.* **47** 69

Takahashi M 1974 *Prog. Theor. Phys.* **52** 71
[15] Frahm H and Korepin V E 1990 *Phys. Rev.* B **42** 10 553
Frahm H and Korepin V E 1991 *Phys. Rev.* B **43** 5653
[16] Keldish L V and Kopaev Yu V 1965 *Sov. Phys.–JETP* **21** 790
Jerome D, Rice T M and Kohn W 1967 *Phys. Rev.* **158** 462
[17] Halperin B I and Rice T M 1968 *Solid State Physics* vol 21, ed F Seitz and D Turnbull (New York: Academic) p 115
[18] Kozlov A N and Maksimov L A 1965 *Sov. Phys.–JETP* **21** 790
Kozlov A N and Maksimov L A 1966 *Sov. Phys.–JETP* **22** 889
[19] Mattis D C 1966 *Rev. Mod. Phys.* **58** 361
[20] Kocharian A N and Khomskii D I 1976 *Sov. Phys.–JETP* **44** 404
Kocharian A N and Khomskii D I 1976 *Solid State Commun.* **18** 985
[21] Takahashi M 1990 *Prog. Theor. Phys.* **43** 917
[22] Schlottman P 1994 *Physica* B **194–196** 1297
[23] Sorella S, Tossati E, Baroni S, Car R and Parrinello M 1988 *Int. J. Mod. Phys.* B **1** 457
[24] White S R, Scalapino D J, Sugar R L, Loh E Y, Gubernatis J E and Scalettar R 1989 *Phys. Rev.* B **40** 506
Shiba H and Pincus P 1972 *Phys. Rev.* B **5** 1966
Dagotto E 1994 *Rev. Mod. Phys.* **66** 763
[25] Hirsch J H 1985 *Phys. Rev.* B **31** 4403
Hirsch J H 1980 *Phys. Rev.* B **35** 5259
Lin H Q and Hirsch J H 1987 *Phys. Rev.* B **35** 3359
[26] Penn D 1966 *Phys. Rev.* **20** 142
[27] Johansson B and Berggren K-F 1969 *Phys. Rev.* **131** 855
[28] Langer W D, Plischke M and Mattis D C 1969 *Phys. Rev. Lett.* **23** 1448
[29] Langer W D and Mattis D C 1971 *Phys. Lett.* A **36** 139
[30] Kimball J C and Schrieffer J R 1972 *Magnetism in Alloys* ed P A Beck and J T Waber (Warrendale, PA: Metallurgical Society of the AIME) p 21
[31] Shiba H 1972 *Prog. Theor. Phys.* **48** 2171
[32] Hubbard J 1963 *Proc. R. Soc.* A **276** 283
Hubbard J 1964 *Proc. R. Soc.* A **281** 401
[33] Cyrot M 1972 *J. Physique* **33** 125
[34] Gutzwiller M C 1965 *Phys. Rev.* **137** 11 726
Gutzwiller M C 1964 *Phys. Rev.* **134** A923
Gutzwiller M C 1963 *Phys. Rev. Lett.* **10** 159
[35] Brinkman W F and Rice T M 1970 *Phys. Rev.* B **2** 4302
[36] Nozières P and Schmitt-Rink S 1985 *J. Low Temp. Phys.* **59** 195
[37] Leggett A J 1980 *J. Physique Coll.* **41** C7 19
Pekalski S and Przystawa J (ed) 1980 *Modern Trends in the Theory of Condensed Matter* (Berlin: Springer) p 13
[38] Micnas R, Ranninger J and Robaszkiewicz S 1990 *Rev. Mod. Phys.* **62** 113
[39] Kocharian A N, Yang C and Chiang Y L 1999 *Phys. Rev.* B **59** 7458
Kocharian A N, Yang C and Chiang Y L 1999 *Int. J. Mod. Phys.* B **29–31** 3538
[40] Randeria M, Trivedi N, Moreo A and Scalettar R T 1992 *Phys. Rev. Lett.* **69** 2001
[41] Kocharian A N, Yang C, Chiang Y L and Kioussis N 1999 *Physica* B **259–261** 739